

AN AXIAL POSITION SENSOR FOR ACTIVE MAGNETIC BEARINGS *

Alexei V. Filatov Lawrence A. Hawkins
Calnetix Inc.
12880 Moore Street, Cerritos, CA 90703

ABSTRACT

Inductive sensors commonly used in Active Magnetic Bearings (AMBs) comprise soft-magnetic cores on stators and sensor targets on rotors. The rotor position is estimated based on values of inductances of sensor coils wound around the cores. These sensors are often easier to use than eddy-current sensors, but their readings can be affected by stray magnetic fields from AMB actuators. For radial sensors this problem can be mitigated by using two diametrically-opposite sensor heads in differential connection, however, the same cannot be done for axial sensors. In addition, the axial sensors often need to be located as close as possible to axial actuators, where the stray fields are higher, in order to minimize changes of the actuator operating gaps caused by differences in thermal expansions of the rotor and the stator.

The axial sensor presented in this paper has been developed to address primarily the issue of sensitivity to external fields. The closest kin of the proposed sensor is the axial inductive edge sensor. Because the magnetic excitation flux in the new sensor is maintained nearly constant during the operation, it was given a name “a constant-flux edge sensor”. A prototype of the new sensor has been built and tested.

Keywords: Position Sensor, Active Magnetic Bearing.

INTRODUCTION

The operational principle of Active Magnetic Bearings (AMBs) [1] requires continuous monitoring of the rotor position with respect to the stator. Even though a significant progress has been made in developing self-sensing AMBs [2], their fundamental performance limitations will likely limit their use to low-cost low-speed machines and a conventional arrangement utilizing dedicated radial and axial sensors will remain dominant. From a wide variety of the available technologies, including optical, capacitive, and electromagnetic position sensors, the latter have received the

widest acceptance due to their robustness, ease of use, and immunity to dust and other contaminations [1]. The electromagnetic sensors fall into two categories: inductive (reluctance) sensors and eddy-current sensors. The inductive sensors [3] utilize a closed magnetic circuit formed by a soft-magnetic, electrically non-conductive stationary core and a sensor target mounted on the object which position is being measured. The stationary core and the sensor target are separated by an air gap. Instead of using a soft-magnetic but electrically non-conductive material, the sensor head cores and the sensor target are often assembled from electrically isolated laminations of electrical steel stuck together in the axial direction. The position measurements are based on measurements of inductances of sensor coils wound around the stationary cores. Changes in the rotor position result in changes of the magnetic reluctance of the air gap, and, consequently, changes in the inductance of a coil wound around the stationary portion of the magnetic circuit. These changes in the inductance are subsequently converted into the sensor output signal by sensor electronics.

The operational principle of the eddy-current sensors [4], [5] is similar to that of the inductive sensors, but the sensor target is made highly-conductive, and preferably, non-magnetic. An AC magnetic flux generated by a sensor coil induces eddy currents in the sensor target, which, in turn, affects the coil inductance. Since this effect depends on the distance between the sensor core and the sensor target, changes in the position of the sensor target result in changes of the coil inductance, similar to the inductive sensors. In order to maximize sensitivity to the target position and simplify the construction, eddy-current sensors in most cases do not have soft-magnetic cores. With no core, and with a non-magnetic target, the inductance of an eddy-current sensor coil is typically a small fraction of an inductance of an inductive sensor. This inductance is further reduced by the presence of the eddy currents. Because of small inductances, in order to obtain a necessary signal-to-noise ratio without exceeding current limits in the sensor coil, the eddy-current sensors are

typically operated at much higher frequencies than the inductive sensors (approximately 500kHz to 2MHz for the eddy-current sensors versus 1 to 100kHz for the inductive sensors). Small inductance of the eddy-current sensors complicates their usage in magnetic bearing systems because the impedance of the wires connecting the sensor coil to the sensor electronics often becomes comparable with the inductance of the sensor coil. As a result any changes to the wires length, adding an additional connector, or even changing how the wires are routed in space may have effect on the sensor readings [5]. Furthermore, electronics for processing higher-frequency signals used by the eddy-current sensors is more complicated and expensive than electronics for the inductive sensors.

Alternative designs of the eddy-current sensors are also known [6], however, while offering the cost and manufacturability advantages they still require very high operational frequency.

Figure 1 shows a typical arrangement of inductive sensors to measure radial displacements of a rotor in X and Y directions. This arrangement includes two sensor heads per

measurement axis located along the axis diametrically opposite to each other in the proximity of the sensor target (for example sensor heads LY2 and LY1 are used to measure the rotor displacement along the Y axis). In one of the common signal processing schemes, shown here as an example, windings of the sensors associated with a particular axis are connected in series forming a voltage divider and energized with an AC voltage of a fixed amplitude. If the sensor target is shifted for example towards the LY2 sensor (positive Y direction), the inductance of this sensor winding will become bigger, whereas the inductance of the sensor winding LY1 will become smaller. As a result, voltage drop on the LY2 sensor winding UY2 will become bigger than the volt drop UY1 on the LY1 sensor. After demodulation, the voltage difference UY2-UY1 can be used as a measure of the rotor displacement in the Y direction.

Both inductive and eddy-current sensors can be used to measure either radial or axial displacements of rotors. For example Figs 2 and 3 illustrate two common ways of using inductive sensors to measure axial displacements.

The arrangement shown in Fig. 2 is almost identical

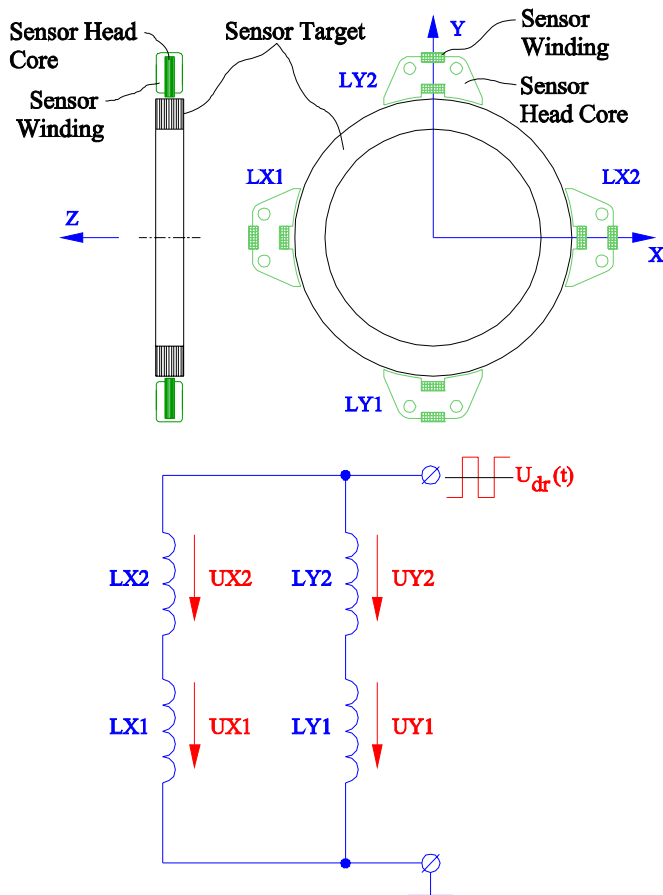


FIGURE 1. AN EXAMPLE OF A CONVENTIONAL ARRANGEMENT OF INDUCTIVE SENSORS TO MEASURE RADIAL DISPLACEMENTS OF A SENSOR TARGET.

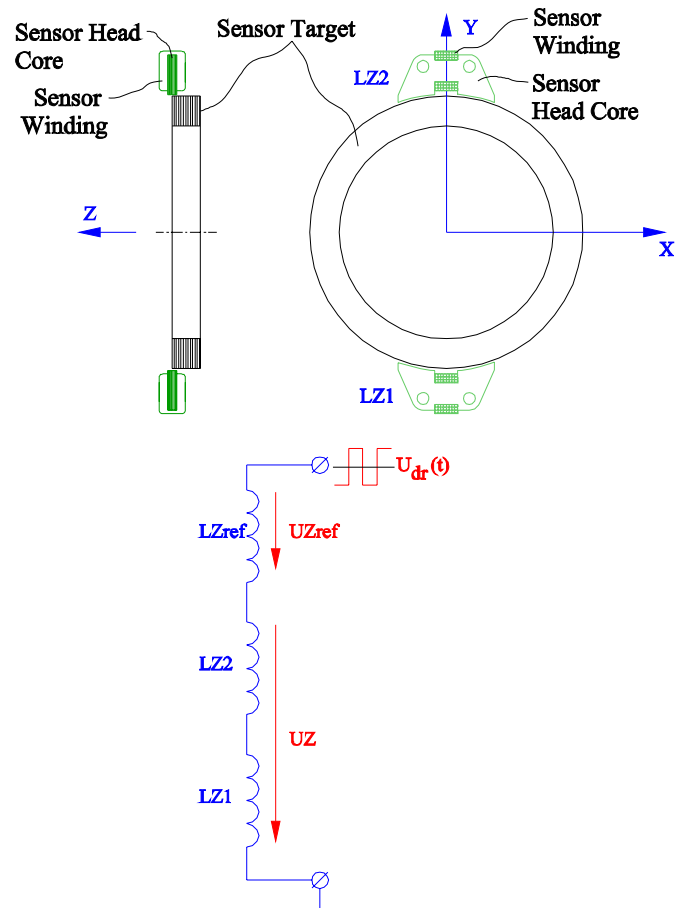


FIGURE 2. AN EXAMPLE OF A CONVENTIONAL ARRANGEMENT OF INDUCTIVE SENSORS TO MEASURE AXIAL DISPLACEMENTS OF A SENSOR TARGET.

to the radial sensor arrangement shown in Fig. 1, but the sensor heads LZ1 and LZ2 are located at an edge of the sensor target rather than in the middle of the target. Because this sensor is effectively monitoring the axial position of the edge of the sensor target it is commonly referred to as an edge sensor. The inductances of two sensor heads LZ1 and LZ2 change synchronously when the rotor moves axially, because this changes the area of overlapping between the sensor head cores and the outer surface of the sensor target. The inductances of individual heads also change when the sensor target is displaced radially in the Y-direction, but they change in the opposite phases. For example, when the sensor target moves in the positive Y direction, the inductance of the sensor LZ2 increases, but the inductance of the sensor LZ1 decreases, and vice versa. Therefore, in the linear approximation, the sum of the inductances LZ1 and LZ2 is not affected by radial displacements of a rotor. In reality, however, changes of the inductances are not linear functions of the radial displacements, and the axial sensors such as shown in Fig.2 exhibit some errors when the rotor is displaced radially. Such errors can be accounted for if the radial position is known, but, nevertheless, this complicates the design.

The lower part of Fig. 2 shows a common signal processing scheme for this type of sensors. It is similar to the signal processing scheme shown for the radial sensors in Fig.1, but the voltage divider is formed by a combination of two sensor inductances LZ1 and LZ2 and an external reference inductance LZref. It is also possible to introduce two more sensor heads LZ3 and LZ4 (not shown) located on the axially-opposite edge of the sensor target from the sensor heads LZ1 and LZ2 and use a combine inductance LZ3+LZ4 instead of LZref in the voltage divider. This arrangement would produce a more linear response than the single-sided arrangement shown in Fig.2, but would be more expensive and would take more axial space.

Figure 3 shows another known method of using an inductive sensor to measure axial displacements of a rotor. In contrast to Fig. 2, the inductance of the sensor head winding in Fig. 3 is changing not because of changes in the area of overlapping between the sensor head poles and the sensor target, but because of changes in the gap between them. Typically the arrangement shown in Fig. 3 offers a higher raw sensitivity than the arrangement in Fig. 2, and no sensitivity to the radial displacements. In practice, however, a higher sensitivity of the sensor shown in Fig. 3 in most cases comes at an expense of a limited bandwidth due to a limitation on the excitation frequency caused by practical difficulties with making the sensor target non-conductive or laminated in the axial plane. Without these measures, the eddy-currents induced in a conductive target will have an effect on the sensor inductance opposite to the effect of changing the air gap in an inductive sensor, resulting in a reduced sensor gain. The higher excitation frequency, the larger would be the eddy-current effect, and the lower would be the sensor gain.

In contrast to the sensor shown in Fig. 2, the sensor shown in Fig. 3 requires a sensor target surface normal to the

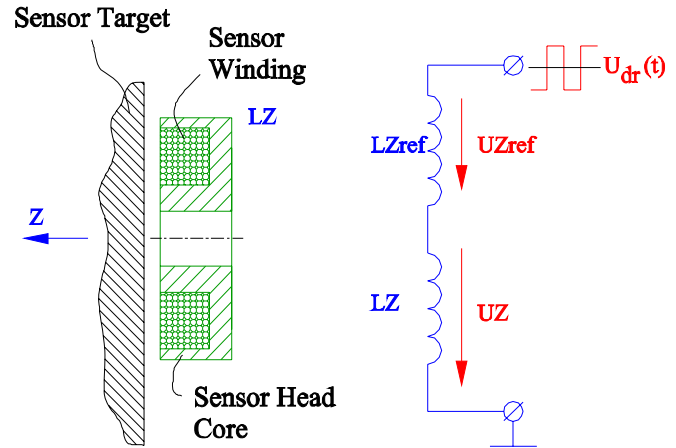


FIGURE 3. ANOTHER EXAMPLE OF A CONVENTIONAL ARRANGEMENT OF INDUCTIVE SENSORS TO MEASURE AXIAL DISPLACEMENTS OF A SENSOR TARGET.

rotor axis Z. If this surface is not readily available, an additional feature has to be added to the rotor, which makes the design more complicated and degrades rotordynamic performance. Moreover, the surface of the sensor target normal to the rotational axis often prone to axial runouts resulting in synchronous and various multiples of synchronous components in the spectrum of the sensor output. This is especially the case when the sensor target is not a part of the rotor, but a separate detachable component mounted on it. An additional advantage of the arrangement shown in Fig. 2 is that it allows a much easier assembly of the machine when the rotor just slides axially with respect to the stator, whereas the sensor target in Fig. 3 makes the rotor insertion possible only in one direction.

As well as in Fig.2, the external reference inductance LZref in the voltage divider in Fig.3 can be replaced with another sensor head located on the axially opposite side of the sensor target. The resulting system would produce a more linear response, but would be more expensive and would take more axial space. In addition, the assembly would become even more complicated, because the sensor target mounted on the rotor will be sandwiched between two sensor heads mounted on the stator.

The arrangement shown in Fig. 3 works as well with an eddy-current sensor instead of the inductive sensor; however the arrangement shown in Fig.2 is much more difficult to realize with eddy-current sensors because the magnetic flux is not guided by soft-magnetic structures, and, therefore, is lacking a well-defined “edge”.

Probably the biggest drawback of the inductive sensors for applications in AMBs is their sensitivity to external magnetic field attracted to the soft-magnetic core of the sensor. Whereas it is typically desirable to locate sensors close to the corresponding actuators to have a more accurate positioning of the actuator target in the nominal position, this

may cause strong magnetic fields produced by the actuator to affect the sensor readings.

Figure 4 illustrates this using an example of a radial or axial edge sensor used in combination with a “Combo” AMB actuator [7] exerting both axial and radial forces on a rotor. The “dashed” line represents a leakage field from the actuator into the sensor. This field affects the operating point of the sensor core material on the BH curve, and, therefore, influences the sensor inductance and, consequently, the position readings. When the axial control flux is varied in order to produce the axial force required from the actuator, the leakage flux varies as well. This results in sensor errors dependent on the axial control current in the actuator.

In the radial sensor arrangement shown in Fig. 1 the effect of the leakage field is mitigated by using two diametrically opposite differentially connected sensor heads: the inductance change for each sensor head due to the leakage field would be the same as the inductance change for the diametrically-opposite head, and, therefore, the output of the voltage divider will not change as long as the rotor is maintained close to the central position. In case of the axial sensors, on the other hand, even if two differentially connected sensors located on the axially opposite sides of the sensor target were used, their changes in the inductance due to the leakage fields will not cancel each other because the sensor heads will be located at different distances from the actuator, and, therefore, will be exposed to different leakage fields. Moreover, the sensor head located closer to the actuator would absorb most of the field, effectively shielding the other sensor head.

The new axial inductive sensor presented in this paper offers the following advantages over existing technologies:

1. Low sensitivity to external leakage fields.
2. Excitation frequency in the ranges where impedance of the external wiring can be neglected, but the sensor bandwidth is sufficient for AMB applications (we used 50kHz excitation frequency).
3. Raw gain above 4.0 V/mm.
4. Very large total measurement range (in excess of 5mm).
5. Sufficiently large linear subranges (at least 0.75mm) where the gain variation does not exceed +/-20%. (There are many linear subranges within the total measurement range).
6. No requirements for a sensor target surface normal to the Z-axis.
7. Commonality with the radial sensor design.

OPERATING PRINCIPLE

The key idea behind the axial sensor design presented in this paper is to use magnetic flux distribution in an air gap rather than the coil impedance as a measure of the axial

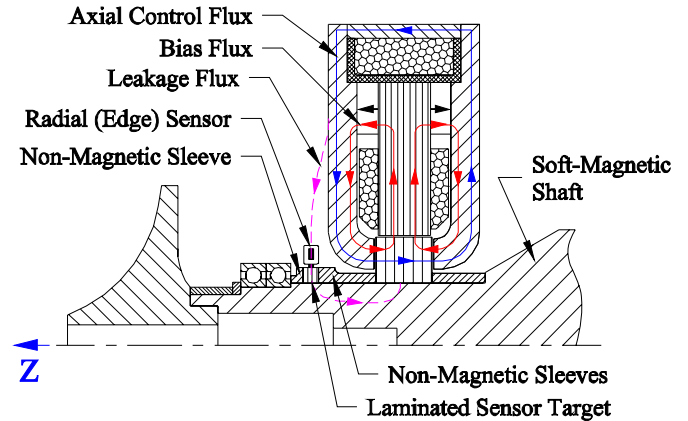


FIGURE 4. AN EXAMPLE OF USING AN INDUCTIVE SENSOR IN AN AMB ILLUSTRATING THE MAGNETIC FLUX LEAKAGE FROM THE ACTUATOR INTO THE SENSOR CORE.

position of the rotor. For example, if we assume that somehow the total magnetic flux in the air gap between a sensor head (e.g. sensor head LZ1) in Fig.2 and the sensor target is maintained constant, then the flux density at each point of the air gap will change when the sensor target is displaced axially. Therefore, by measuring flux density at a certain point, or an average flux density over a certain part of the air gap, one could estimate the axial displacement of the rotor. Figure 5 further clarifies this idea. The total flux injected into the air gap between the sensor head core and the sensor target is represented by five flux lines and is maintained constant regardless the axial position of the sensor target (how to implement this constant-flux requirement will be discussed later). As shown in Fig. 5, the flux density above the actuator target changes when the target is displaced axially from the nominal position shown in Fig. 5a: the space between the flux lines gets smaller (flux density gets higher) when the sensor target moves in the negative Z direction (Fig.5b) and, conversely, the space between the flux lines gets larger (flux density gets lower) when the sensor target moves in the positive Z direction (Fig.5c). This flux density can be measured by inserting a Flux Density Sensing (FDS) Coil into the air gap as shown in Fig.5: the amplitude of the voltage induced on the coil terminals will be proportional to the amplitude of the flux linked to the coil, which, in turn, will be proportional to the flux density in the area of interest. For example, with the sensor target in the nominal position (Fig. 5a), there are three flux lines linked to the FDS Coil. If the rotor is displaced in the negative Z-direction (Fig. 5b), the number of the flux lines linked to the coil increases to four, and, conversely, if the rotor is displaced in the positive Z-direction (Fig. 5c), the number of the flux lines linked to the coil reduces to two.

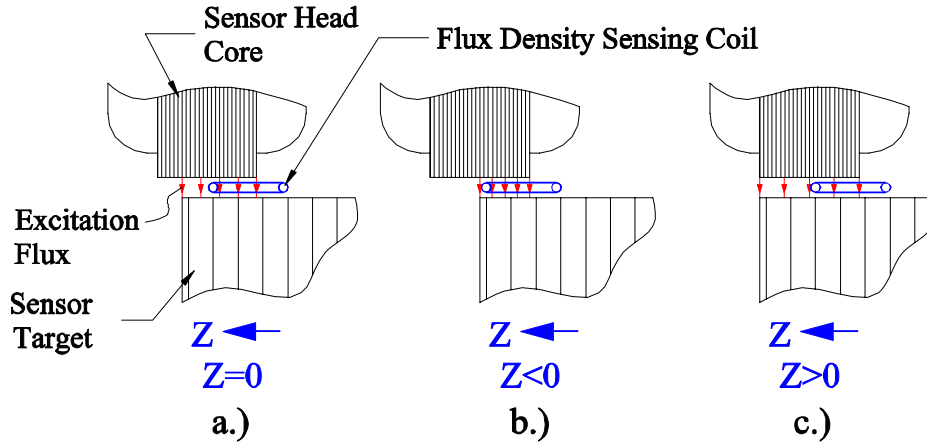


FIGURE 5. ILLUSTRATION OF THE OPERATIONAL PRINCIPLE OF THE CONSTANT-FLUX EDGE SENSOR.

Figure 6 provides more details of the sensor construction and operation. In addition to soft-magnetic and electrically non-conductive Sensor Target Portion #1, it may also have a non-magnetic and electrically conductive Sensor Target Portion #2. An AC magnetic flux will be expelled from the Sensor Target Portion #2 due to the skin effect and concentrated in the Portion #1, forming a sharp flux edge at the boundary between the two portions. Figure 7 clarifies how the total excitation flux in the air gap is maintained constant. Figure 7a shows an equivalent electrical schematic for the excitation magnetic circuit of the sensor shown in Fig.6. An excitation current $i_{exc}(t)$ flowing in the excitation coil of the sensor comprising N turns creates a magnetomotive force (MMF) $N \cdot i_{exc}(t)$, and, subsequently, induces a magnetic flux $\Phi_{exc}(t)$. The flux path is composed of the sensor head core, radial air gap and sensor target with associated magnetic reluctances R_{head} , R_{gap} and R_{target} respectively.

Figure 7b shows an electrical schematic used to induce the current $i_{exc}(t)$. In contrast to electrical schematics shown in Figs. 1, 2 and 3, there are no voltage dividers involved and the sensor excitation coil is directly connected to a source of excitation voltage $U_{exc}(t)$. Any periodic time profile of the voltage $U_{exc}(t)$ can be used, such as square-wave, triangular, sinusoidal, etc, however the square-wave appears to be the most practical choice. According to Faraday's law, the excitation magnetic flux $\Phi_{exc}(t)$ and the excitation voltage $U_{exc}(t)$ are linked by the following equation:

$$U_{exc}(t) = N \frac{d\Phi_{exc}(t)}{dt} \quad (1)$$

An important outcome of a direct relation between $\Phi_{exc}(t)$ and $U_{exc}(t)$ is that if we maintain the amplitude of $U_{exc}(t)$ constant, then the amplitude of $\Phi_{exc}(t)$ will also stay constant regardless of values of R_{head} , R_{gap} and R_{target} , which can be affected by the external fields, changes in the radial gap,

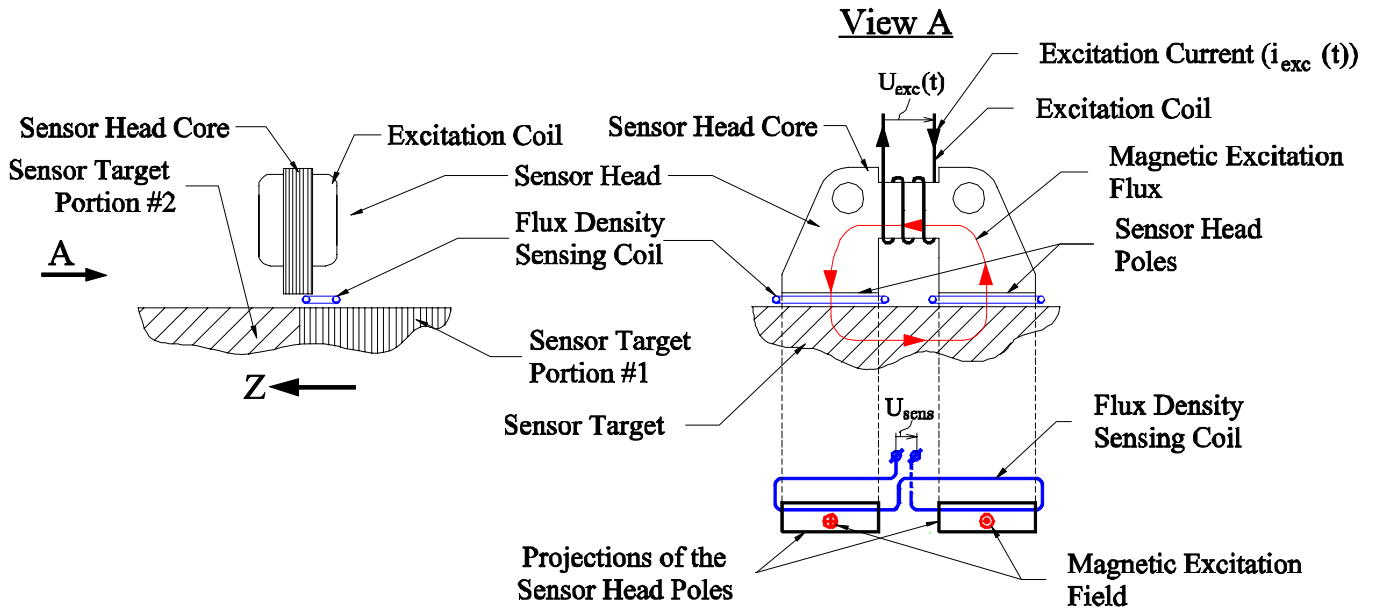


FIGURE 6. DETAILS OF THE OPERATION OF THE CONSTANT-FLUX EDGE SENSOR.

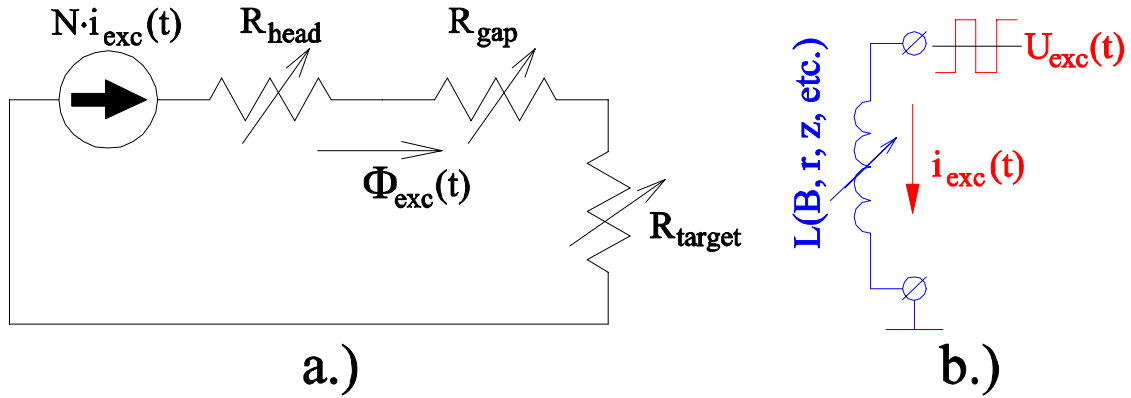


FIGURE 7. EQUIVALENT ELECTRICAL SCHEMATIC FOR THE MAGNETIC CIRCUIT (LEFT) AND AN ELECTRICAL SCHEMATIC FOR THE EXCITATION COIL (RIGHT).

etc. R_{head} , R_{gap} and R_{target} will, however, affect the value of the excitation current $i_{exc}(t)$ – the larger total value of the magnetic reluctance $R_{total} = R_{head} + R_{gap} + R_{target}$, the larger will be the amplitude of the excitation current. This can be also explained using a definition of the inductance of the excitation coil:

$$L = \frac{N \cdot \Phi_{exc}}{i_{exc}} = \frac{N^2}{R_{head} + R_{gap} + R_{target}} \quad (2)$$

Using (2), equation (1) can be presented in a well known form:

$$U_{exc}(t) = L \frac{di_{exc}(t)}{dt} \quad (3)$$

where the inductance L changes when the air gap changes, or when the sensor target is displaced axially, or when the reluctance of the sensor head core changes because of an external magnetic field. For example, when the radial air gap between the sensor head core and the sensor target increases, the reluctance of the gap R_{gap} increases as well, the inductance of the excitation winding L decreases according to (2) and the amplitude of the excitation current $i_{exc}(t)$ increases according to (3). The amplitude of the excitation flux $\Phi_{exc}(t)$, however, will remain constant driven by (1). Because of this feature the new sensor was given a name “a constant-flux edge sensor”.

Because the Sensor Target Portion #1 shown in Fig. 6 can be made laminated, even at high operational frequencies there will be no significant eddy currents induced in it, which would otherwise negatively impact the sensor gain. Moreover, using a higher frequency may even result in a slightly higher gain because the fields would be better expelled from the conductive and non-magnetic Sensor Target Portion #2 producing a better “edge”. This is a big advantage over the sensor shown in Fig.3 where the sensor target is difficult to laminate and eddy currents induced in it result in a loss of the sensor gain at higher frequencies. Even though the sensor bandwidth is also affected by the signal processing electronics,

a higher operational frequency of a sensor allows for a higher sensor bandwidth. Most AMB applications require sensor bandwidth in order of 3kHz, which is very easy to achieve and even exceed with the proposed sensor technology.

SENSOR PROTOTYPE

A prototype of the constant-flux edge sensor has been built and tested. The sensor assembly included two sets of sensor heads and FDS Coils located diametrically opposite from each other with the excitation windings connected in parallel and connected to a source of the excitation voltage of a constant amplitude U_{exc} , whereas two FDS Coils were connected in series so that the voltages induced in them add to each other. The FDS Coils have been manufactured using Flexible PCB technology with a Kapton substrate. This technology is widely used in commercial products (e.g. to manufacture flexible ribbon cables), which makes FDS Coils very inexpensive. The traces on a Flexible PCB can easily be made as small as $75\mu\text{m}$ (0.003in) wide with a $75\mu\text{m}$ gap between them, which allows placing a very large number of turns per unit length. Since there is no current in the FDS coils, a high resistance due to a small cross-section of the traces is not important. An FDS coil manufactured with flexible PCB technology can be easily bent and glued to the inner diameter of the sensor assembly using an appropriate epoxy. Figure 8 shows an FDS coil used in the sensor prototype.

SENSOR TEST RIG

A test rig shown in Fig. 9 has been developed for evaluating the sensor performance, in particular, its sensitivity to external magnetic fields. The external field was generated by permanent magnets mounted on the Field Adjustment Disk. The magnetic circuit for the external field generation included Permanent Magnets, cylindrical Outer and Inner Poles, Sensor Head Core, Sensor Target, Soft-Magnetic Portion of the Rotor, Inner Pole and the Magnetic Backiron. The Field Adjustment Disk was mounted on a threaded rod so that the gap between

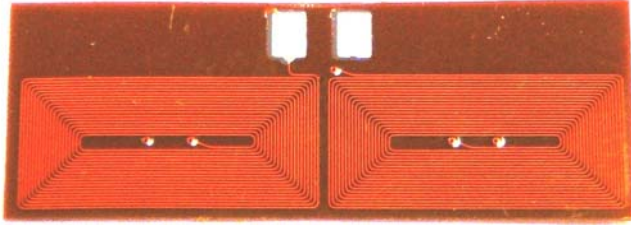


FIGURE 8. FLUX DENSITY SENSING (FDS) COIL MANUFACTURED WITH PCB TECHNOLOGY. THE PCB DIMENSIONS: 29mm × 10mm × 0.38mm (1.14in × 0.41in × 0.015in). THE COIL COMPRISES 156 TURNS (COUNTING TURNS UNDER BOTH SENSOR HEAD POLES).

the disk and the outer and inner poles, and, consequently, the external magnetic field in the sensor heads could be changed by turning the disk. The rotor mockup was mounted on an X-Y table allowing it to be moved axially (Z-direction) and horizontally (X-direction). Note that the sensor heads in Fig. 9 are shown mounted in the vertical plane in order to make them visible in the vertical cross-section, whereas in reality they were mounted in the horizontal plane and moving the rotor mockup in the X-direction was affecting clearances between the sensor heads and the sensor target.

EXPERIMENTAL RESULTS

A prototype of the constant-flux edge sensor exhibited a very large range of the target positions where the sensor output was changing monotonically with the target displacements (in excess of 5mm). The sensor output (after signal processing electronics) as a function of the sensor target position is shown in Fig. 10. In the middle section of the curve shown in Fig. 10, the raw sensor gain defined as change of the RMS voltage measured directly on the terminals of two FDS

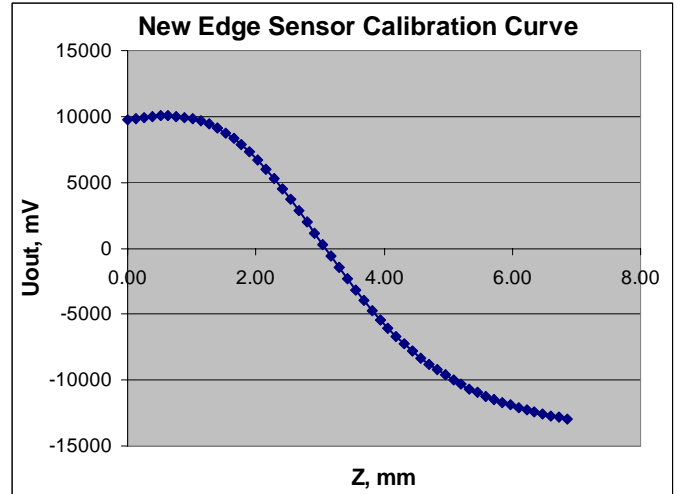


FIGURE 10. SENSOR OUTPUT AFTER SIGNAL PROCESSING ELECTRONICS AS A FUNCTION OF AN AXIAL SENSOR TARGET POSITION.

coils connected in series was in excess of 8V/mm (200V/in). With $\pm 0.38\text{mm}$ ($\pm 0.015\text{in}$) displacement range from the nominal position, the new sensor offers a large range of nominal positions where the gain variations do not exceed 20%.

Probably the most important test was sensitivity to external magnetic fields. Figure 11 shows axial position measurement errors caused by external fields for several axial and radial positions of the sensor target. The field values indicated in Fig. 11 have been measured with a Hall sensor inserted in the air gap between the sensor head poles and the sensor target. The errors observed with a conventional edge sensor utilizing the same sensor heads and tested on the same test rig are also shown for the comparison purposes. More than 20-time reduction of the error in high magnetic fields has been observed with the new constant-flux edge sensor compared to the conventional edge sensor.

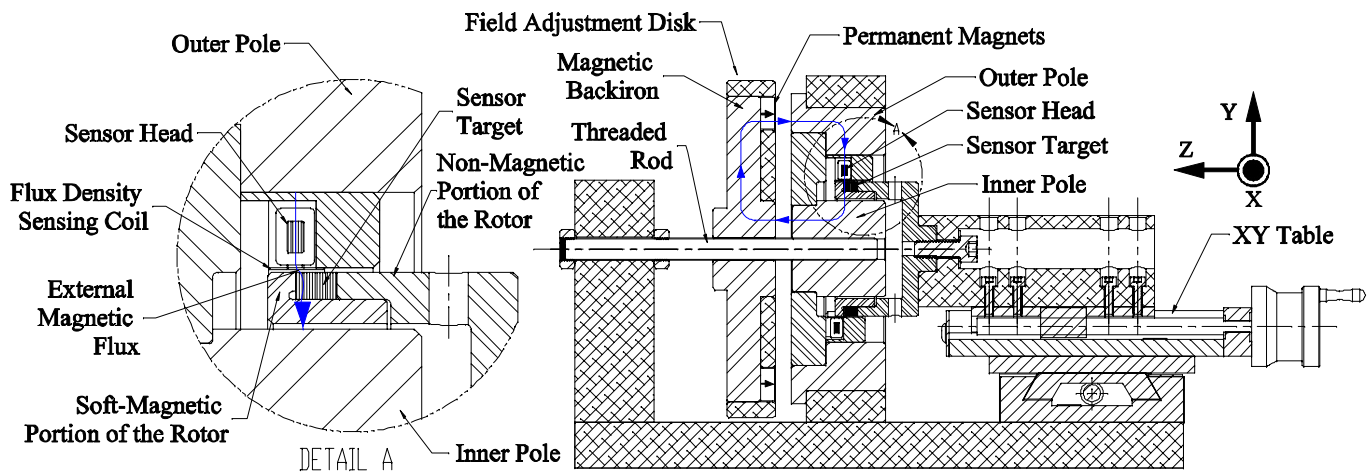


FIGURE 9. TEST RIG USED TO EVALUATE THE SENSOR PERFORMANCE. THE SENSOR HEADS WERE LOCATED IN A HORIZONTAL PLANE, BUT SHOWN IN THE VERTICAL PLANE TO MAKE THEM VISIBLE IN THE VERTICAL CROSS-SECTION.

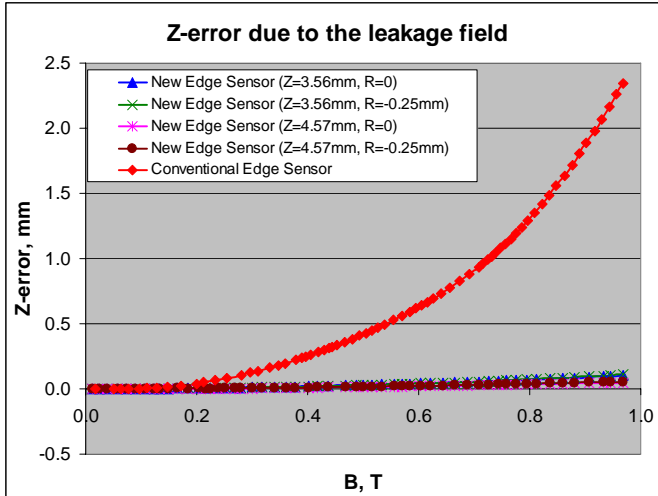


FIGURE 11. ERROR IN MEASUREMENT OF THE AXIAL SENSOR TARGET POSITION DUE TO AN EXTERNAL MAGNETIC FIELD B.

Figure 12 illustrates another error, caused by rotor radial displacements. As mentioned earlier, this error in the conventional edge sensors can be corrected based on the radial sensor readings, however, having a much smaller error in the constant-flux edge sensor eliminates the need for such corrections and simplifies the system design. An asymmetric character of this error for the constant-flux edge sensor indicates that it originates from differences in properties of two diametrically opposite sensor head – FSD coil assemblies.

CONCLUSIONS

A new design of an axial position sensor (constant-flux edge sensor) has been proposed and evaluated. The main advantage of the new sensor compared to existing inductive

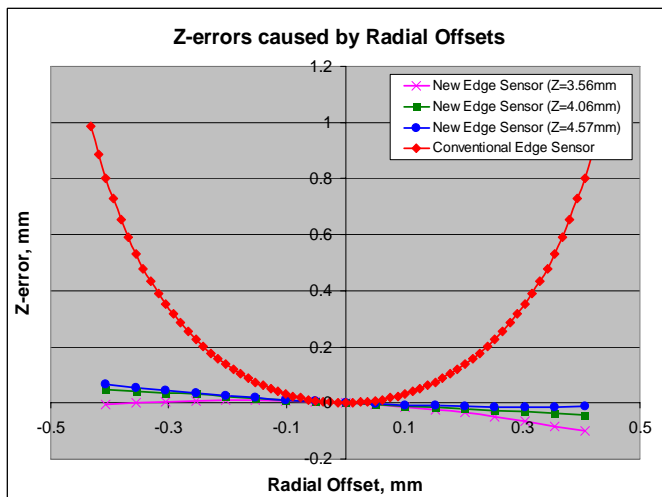


FIGURE 12. ERROR IN MEASUREMENT OF THE AXIAL SENSOR TARGET POSITION DUE TO RADIAL TARGET DISPLACEMENTS.

edge sensors is a significantly lower sensitivity to external magnetic fields. This feature is particularly beneficial for applications in Active Magnetic Bearings (AMBs), because it allows locating the sensor close to an AMB where it may be exposed to strong magnetic fields leaking out from an actuator.

The sensor has been recently integrated into a commercial machine on magnetic bearings - a 165kW 26.5kRPM Expander/Generator for Waste Heat Recovery [8], which has been successfully tested at full operating speed. The sensor is also scheduled to be integrated into a 330kW 32kRPM gas compressor on magnetic bearings.

NOMENCLATURE

Symbol	Meaning
B	Magnetic Flux Density
i	Current
L	Inductance
N	Number of Turns
R	Magnetic Reluctance
U	Voltage
Φ	Magnetic Flux

REFERENCES

- [1] Editors: Schweitzer, G., Maslen, E. H., 2009, Magnetic Bearings, Springer-Verlag, Berlin Heidelberg.
- [2] Maslen E.H., Iwasaki T., Mahmoodian, R., 2006, "Formal Parameter Estimation for Self-Sensing", Proc. 10th International Symposium on Magnetic Bearings, Martigny, Switzerland.
- [3] Moriyama, S, Katsuhide, W., Takahide, H, 1998, "Inductive Sensing System For Active Magnetic Suspension Control", Proc. 6th International Symposium on Magnetic Bearings, Massachusetts, USA, pp. 529-537.
- [4] Li, L., 2008, "Eddy-Current Displacement Sensing Using Switching Drive When Baseband Sensor Output Is Readily Available", IEEE Transactions on Instrumentation and Measurement, Vol. 57, No. 11, pp. 2548-2553.
- [5] www.kamansensors.com/html/technology/technology-technology-cablelength.htm
- [6] Larsonner, R., Buhler, P., 2004, "New Radial Sensor for Active Magnetic Bearings", Proc. 9th International Symposium on Magnetic Bearings, Lexington, Kentucky, USA.
- [7] McMullen, P. T., Huynh, C. S., and Hayes R. J., 2000, "Combination Radial-Axial Magnetic Bearing", Proc. 7th International Symposium on Magnetic Bearings, ETH, Zurich, Switzerland, pp. 473-478.
- [8] Hawkins L. A., Zhu L., Blumber, E. J., 2010, "Development of a 125kW Expander/Generator for Waste Heat Recovery", Proc. of ASME Turbo Expo 2010: Power for Land, Sea and Air, Glasgow, UK.